University College Dublin

Thesis

Development and validation of a particle-based model of electroporation.

Author:
Peter Murphy, 16440004

Supervisor:
Prof. P. Ballone

This thesis is submitted to University College Dublin in partial fulfilment of the requirements for the degree of BSc in Theoretical Physics

in the

School of Physics

April 24, 2020

Abstract

The response of a model that reproduces the bilayer structure of a lipid membrane to an external electric field at different temperatures is investigated by Monte Carlo simulations. The model is based on particles that carry a dipole of constant length where the potential between two particles is the sum of a spherical pair interaction and a dipole-dependent term. This last contribution is similar to the electrostatic dipole-dipole interaction, with, however, a change of sign that modifies the orientation dependence of the interaction. Then, the minimum energy configuration of this model has the dipoles in each leaflet parallel amongst themselves and anti-parallel to the dipoles in the other leaflet. In this way, the ground state of the system consists of a bilayer of particles, whose geometry and properties mimics those of lipid bilayers. The simulation results show that in the absence of the electric field, the bilayer is very stable for a range of temperatures. The model displays a 2D solid-liquid transition, representative of the transition seen in real biomembranes. When the electric field is applied, the leaflet with dipoles anti-parallel to the electric field becomes destabilized, forming holes in the leaflet. This phenomenon is similar to electroporation, however it is not observed in the leaflet with dipoles parallel to the electric field, although the source of this problem is known and will be easily corrected.

Contents

List of Figures

Acknowledgements
I would like to thank Prof. Pietro Ballone for all his help during the planning and development of this experiment. His willingness to give his time so generously has been very much appreciated.

Declaration of Authorship
I declare that all material in this assessment is my own work except where there is clear acknowledgement and appropriate reference to the work of others.

1 Introduction

Electroporation is a widely used biophysical method to increase the permeability of the biomembrane that surrounds biological cells through the application of electric pulses. The technique has been developed and is currently used to introduce genetic material such as DNA or RNA segments into cells, whose delivery would otherwise be prevented by the biomembrane. The increase of permeability, that can be permanent or more often transient, is caused by a change of the electrostatic potential across the membrane of the order of a Volt. The basic principles of the phenomenon are known, and can be explained in simple terms. The biomembrane, consisting primarily of a phospholipid bilayer with the addition of proteins and saccharides, represents a dielectric layer of nanometric (typically 4 nm) thickness embedded into an electrically conducting fluid consisting of a water solution of electrolytes. The dielectric signature of the bilayer is due to the polar (sometimes ionic) character of phospholipids, whose hydrophilic head carries a permanent electric dipole. The application of the external field changes the electrostatic equilibrium of the system, disrupting the integrity and thus the impermeability of the biomembrane. Beyond this simple picture, a wide variety of details and microscopic mechanisms of electroporation remain elusive because of the non-linear character of the phenomenon, and also because of its stochastic character. The experimental evidence shows that electroporation takes place as an activated transformation, whose nucleation is difficult to predict. The disruption caused by electroporation is locally very large, well beyond the reach of perturbation theory and linear analysis, greatly enhancing the difficulty of finding a quantitative description.

In the last decades, computational methods and computer simulation in particular have added one more option to analyse the properties and evolution of com-

plex systems, up to the size and complexity of biosystems. Up to now, however, the contribution of simulation to the understanding of electroporation has not been overwhelming, because of the variety of size and time scales involved in this phenomenon. By contrast, and apart from a few exceptions, simulation based on atomistic models is limited to sizes of the order of 100 nm, and time scales of the order of 100 ns, still orders of magnitude below the 20 μm and 10μs scales of electroporation.

To ease the task of addressing electroporation by computer simulation, this project aims at developing and validating a simplified model of this phenomenon, able to increase the reach of simulation by at least an order of magnitude in size and time, approaching the regime relevant for electroporation. To exploit the standard machinery of simulation, the model has to be based on particles. To extend the reach of simulation, the model has to be heavily coarse-grained, i.e., it has to represent molecules by a single particle, and it has to include the solvent (water) only in an implicit way. These choices will limit the resolution of the method, but will greatly increase its scope.

The model development takes its origin from a model of lipid bilayers proposed in the literature a few years ago[1]. The development stage added several details to the model, deemed necessary to reproduce electroporation. The validation of the model has relied on a series of simulations, showing that the project aim has been achieved to a large extent, although a few details still need to be incorporated or improved.

2 Experimental Picture

The cell membranes of almost all organisms are made of a lipid bilayer. The lipids have a polar, hydrophilic head and neutral, hydrophobic tail, so they arrange

themselves in a bilayer when in contact with water. This allows them to perform their function of regulating what molecules enter and leave the cell. Electroporation is the reversible process of applying an external electric field in short pulses to a cell membrane, causing aqueous pores to form, increasing the permeability of the membrane. In the 1980s, labs began using this method to introduce otherwise impermeable molecules into cells[2]. Since then, the method has been widely used in biology, biotechnology and medicine, however, the underlying mechanism of pore formation is still not fully understood. Both theoretical considerations and molecular dynamics simulations imply that electroporation is initiated by penetration of water molecules into the lipid bilayer of the membrane[3], which causes the lipids to rearrange so that the polar heads remain in contact with the water, forming meta-stable pores. Most cell's maintain a potential difference between

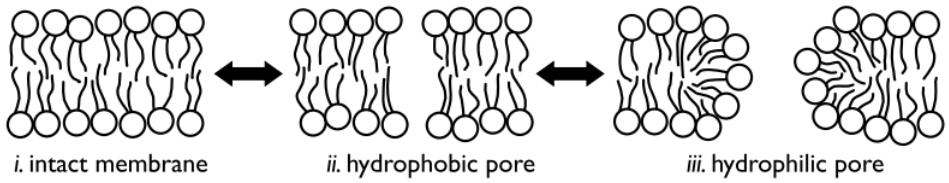

Figure 1: Lipid bilayer before and after application of an electric field.[4]

the inner and outer layers of their membrane, called the transmembrane voltage (TMV), usually in the range of -40mV to -70mV, with the inner potential lower than the outer potential[5]. Applying an external transmembrane electric field to the cell increases the TMV, causing a number of biophysical and biochemical changes to the membrane and its constituent molecules. The most prominent of these changes is electropermeabilization - a large increase in membrane permeability, and the main process by which this happens is electroporation. Early experiments showed that electroporation occurs only when a critical value of TMV is reached. As the pores formed by electroporation are nanometres in size, they are

too small to be observed by optical methods, and they are too fragile to be observed by electron microscopy of soft matter. Therefore, visualizing the dynamics of pore formation is very difficult. However, molecular dynamics simulations have shown promising results in describing pore formation[6,7].

3 Theoretical Models

There have been a number of theoretical models used to try and describe the mechanisms of electroporation. The ideal model should contain,

(1) A physically realistic picture of the membrane before and after breakdown,

(2) Dependence on the number of pulses and their amplitude and duration. Longer pulses require a lower amplitude to achieve permeabilization.

(3) Depending on the pulse parameters, the process is reversible or irreversible.

(4) A value for the critical TMV, usually as a function of model parameters, in agreement with experimental measurements of hundreds of millivolts.

(5) A certain degree of stochasticity is observed in electropermeabilization of pure lipid vesicles and planar bilayers. Some authors view the ability of a model to account for this as crucial[8].

The hydrodynamic model[9,10], the elastic model[11] and the viscohydroelastic model[12,13] view electroporation as a large scale phenomenon where the molecular structure of the membrane is insignificant. They treat the membrane as a charged layer of a non-conductive liquid separating two conductive liquids. The TMV exerts a pressure on this layer. In the hydrodynamic case, the volume of the layer is assumed constant and the surface area increases, causing an increase in the pressure due to surface tension opposing the compression. The membrane perimeter is assumed constant, causing the membrane to ripple. In the elastic case, the area is assumed constant and the volume decreases, causing an increase

in the elastic pressure opposing the compression. When the TMV reaches a critical value, the pressure can no longer maintain equilibrium, and breakdown occurs. The viscohydroeleastic combines these two, including both the surface tension and elasticity, varying both the volume and area, and also includes the membrane viscosity which causes the compression to happen gradually after the TMV is applied, not instantaneously. The hydrodynamic model gives a realistic value for the critical TMV but the elastic and viscohydroelastic do not, and they all fail to meet any of the other requirements listed, except for the viscohydroelastic providing a link between the critical TMV and a critical pulse duration.

The phase transition model[14] takes a different approach and looks at the interactions between individual lipid molecules. Instead of membrane pressure, molecular free energy is considered, with several minima of the free energy corresponding to stable states. The free energy of a membrane with average molecular surface area S, temperature T an applied TMV is given by[8],

$$W(T,S) = W_f(S) + W_c(T,S) + W_{ic}(T,S) + W_{ih}(T,S) + W_e(T,S,U) \qquad (1)$$

where W_f is the flexibility energy (from continuous deformations), W_c is the conformational energy (from discrete deformations), W_{ic} is the energy of interactions between the hydrocarbon chains, W_{ih} is the energy of interactions between the polar heads of the lipids and W_e is the electrical energy.

Unfortunately, only W_f and W_e have a real physical basis, so this model doesn't give a meaningful value for the critical TMV. However, it does meet some of the requirements which the previous models didn't. The membrane before and after permeabilization corresponds to different minima in the free energy. The energy input required for this change could explain the dependence on the pulse duration, and above a second critical potential shown in Fig. 2, there is no second minima,

which could explain the limited reversibility.

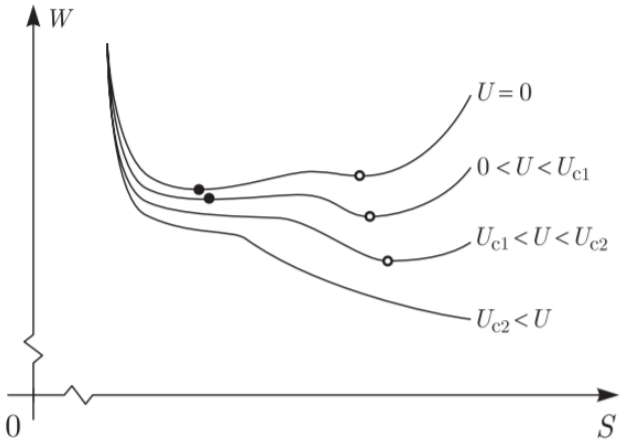

Figure 2: Free energy of a lipid molecule in the bilayer as a function of the molecular area, at four different TMVs. The units on both axes are arbitrary.[8]

The aqueous pore formation model, described in the previous section, offers a compromise between these two approaches, and is considered the most realistic model at this time.

4 Preliminary Study

Bingham[15] offered a method to model the response of a lipid bilayer to an external electric field, using a free energy functional. The model contains a continuum description of the membrane dipoles with a coupling of their spin orientations with the membrane surface tilt. When the electric field is applied, the heads try to align with it, causing the membrane to become unstable. A free energy functional is constructed to analyse this instability. There are six contributions to the free energy, f_m for the mechanical deformation of the membrane, f_d for the dielectric energy, f_p for tilting of the dipoles relative to the membrane, f_χ for changes in dipole alignment, f_c for coupling the dipole alignment with the surface curva-

ture and $f_{E_{A,B}}$ for two uncoupled dipoles in an electric field.

$$f_m = \frac{\kappa_b}{2}(h''_+ + h''_-) + \frac{\gamma}{2}(h'_+ + h'_-) + \frac{\kappa_A}{2}\left[\left(\frac{t_+}{t_0} - 1 - t_0 s''\right)^2 \left(\frac{t_-}{t_0} - 1 + t_0 s''\right)^2\right], \quad (2)$$

$h_\pm$ = position of upper and lower membrane surfaces, $t_\pm$ = thickness of upper and lower membrane leaflets, t_0 = unperturbed monolayer thickness, s = displacement of the dividing surface between the monolayers, κ_A = compressibility modulus, κ_b = bending rigidity, γ = surface tension.

$$f_d = \frac{\epsilon_0}{2}[\epsilon_m E_m^2(h_+ - h_-) + \epsilon_w E_+^2(L - h_+) + \epsilon_w E_-^2(h_- - L)], \quad (3)$$

$\epsilon_0, \epsilon_m, \epsilon_w$ = dielectric constant of the vacuum, membrane, water, E_m = field in the membrane, $E_\pm$ = field at the upper and lower membrane surface, L = upper and lower limit of the system. The dipolar headgroups of the lipids are defined by the vector $\mathbf{p}$;

$$\mathbf{p} = \mathbf{p}_z + \mathbf{m} = pcos(\theta)\hat{e}_z + \mathbf{m} \quad (4)$$

θ = angle the dipole makes with the z direction, $\mathbf{m}$ = vector representing the in-plane dipole moment. Perturb about the equilibrium position; $\theta_\pm = \theta_{0\pm} + \delta\theta_\pm$, where $\theta_{0+} = \theta_0,\ \theta_{0-} = \pi \pm \theta_0$ (for A and B).

$$f_p = \frac{\kappa_p(\mathbf{m}_+ \cdot \hat{e}_x)^2}{2}(\delta\theta_+ + h'_+)^2 + \frac{\kappa_p(\mathbf{m}_- \cdot \hat{e}_x)^2}{2}(\delta\theta_- + h'_-)^2, \quad (5)$$

κ_p = the dipole-membrane coupling modulus. To treat larger membrane areas, change $\mathbf{p}$ and $\mathbf{m}$ from single dipole to continuum variables. $\mathbf{p}$ becomes a dipole moment density $\tilde{p}$. We coarse grain $\mathbf{m}$ into $\bar{\mathbf{m}} \equiv \langle \mathbf{m} \rangle$, the average orientation of dipoles within a small area. Write $\tilde{m} = |\bar{\mathbf{m}}|$, set $\hat{m} = \hat{e}_x$ and allow $\tilde{m}$ to vary, $\tilde{m}_\pm = \tilde{m}_0 + \delta\tilde{m}_\pm$. Changes in dipole alignment are penalized by a susceptibility

χ_m, giving f_χ by,

$$f_\chi = \frac{\chi_m}{2}\delta\tilde{m}_\pm^2. \tag{6}$$

$$f_c = -\frac{\gamma_c}{2}[h''_+\delta\tilde{m}'_+ + h''_-\delta\tilde{m}'_-], \tag{7}$$

γ_c = the dipole alignment-membrane coupling.

$$f_{E_{A,B}} = \tilde{p}E\left[\frac{cos(\theta_0)}{2}(\delta\theta_+^2 - \delta\theta_-^2) + sin(\theta_0)(\delta\theta_+ \mp \delta\theta_-)\right]. \tag{8}$$

Assuming $E_+ = E_- = E$.

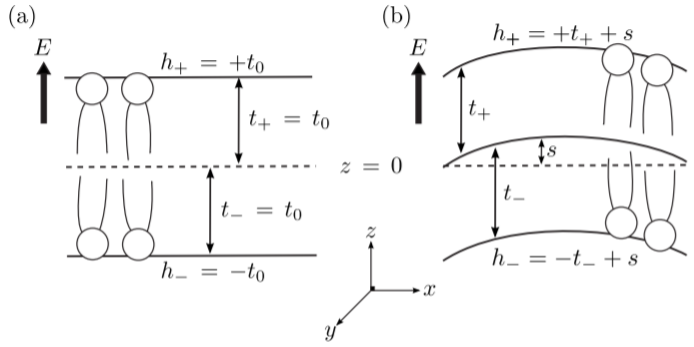

Figure 3: (a) Unperturbed bilayer and (b) deformed bilayer.[15]

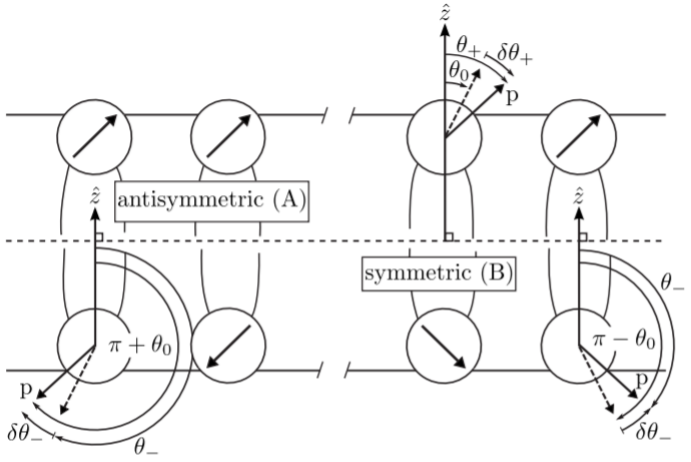

Figure 4: Symmetric and antisymmetric orientations.[15]

After a change of variables, $u = h_+ - h_-$ (peristaltic mode), $\bar{h} = h_+ + h_-$ (bilayer mode), $\Delta = \delta\theta_+ - \delta\theta_-$ (difference in dipole tilts), $\Sigma = \delta\theta_+ + \delta\theta_-$ (mean dipole tilt), then minimizing with respect to Δ and Σ, then expanding u and $\bar{h}$ as small perturbations, $u = u_0 + \delta u$ and $\bar{h} = \bar{h}_0 + \delta\bar{h}$, the free energy is, $f = f_0(u_0, \bar{h}_0) + \delta f(\delta u, \delta\bar{h})$, and the stability of the system is determined by δf,

$$\delta f = \frac{\kappa_b}{4}(\delta u''^2+\delta\bar{h}''^2)+\frac{\gamma}{4}(\delta u'^2+\delta\bar{h}'^2)+\frac{\kappa_A}{2t_0^2}\left(\frac{\delta u^2}{2}\right)-\frac{\gamma_c}{4}[(\delta\bar{h}''+\delta u'')\delta\tilde{m}'_+ +(\delta\bar{h}''-\delta u'')\delta\tilde{m}'_-]$$

$$+\frac{\chi_m}{2}(\delta\tilde{m}_+^2+\delta\tilde{m}_-^2)+\frac{[\kappa_p^3\tilde{m}_0^6(\delta\bar{h}'^2+\delta u'^2)-2\kappa_p^2\tilde{m}_0^4\tilde{p}E\cos(\theta_0)\delta u'\delta\bar{h}']}{4[\kappa_p^2\tilde{m}_0^4-\tilde{p}^2E^2\cos^2(\theta_0)]}. \qquad (9)$$

Which is then decomposed into Fourier modes,

$$\delta u = \sum_q u_q t_0 e^{-i\hat{q}x/t_0},\ \delta\bar{h} = \sum_q \bar{h}_q t_0 e^{-i\hat{q}x/t_0},\ \delta\tilde{m}_\pm = \sum_q \tilde{m}_q^\pm t_0 e^{-i\hat{q}x/t_0},$$

So,

$$\delta f = \frac{L^2}{(2\pi)^2}\frac{\kappa_b}{2t_0^4}\sum_q \delta f_q,$$

$$\delta f_q = \frac{1}{2}\left[\hat{q}^4+\left(\sigma_s-\sigma_p\frac{\phi^2}{\sigma_p^2-\phi^2}\right)\hat{q}^2\right](|\bar{h}_q|^2+|u_q|^2)+\frac{\sigma_A}{2}(|u_q|^2)+\sigma_p^2\hat{q}^2\frac{\phi^2}{\sigma_p^2-\phi^2}(\bar{h}_q^*u_q+\bar{h}^*u_q^*)$$

$$+\sigma_\chi(|\delta\tilde{m}_q^+|^2+|\delta\tilde{m}_q^-|^2)+\frac{i\sigma_c\hat{q}^3}{2}[(\bar{h}_q^*+u_q^*)\delta\tilde{m}_q^+ +(\bar{h}_q^*-u_q^*)\delta\tilde{m}_q^-]. \qquad (10)$$

$$\sigma_p = \frac{\kappa_p\tilde{m}_0^2t_0^2}{\kappa_b},\ \sigma_s = \frac{\gamma t_0^2}{\kappa_b},\ \sigma_A = \frac{\kappa_A t_0^2}{\kappa_b},\ \sigma_\chi = \frac{\chi_m t_0^2}{\kappa_b},\ \sigma_c = \frac{\gamma_c}{\kappa_b},\ \phi = \frac{\tilde{p}Ecos\theta_0 t_0^2}{\kappa_b}.$$

We can rewrite Eq .9 in matrix form, whose eigenvalues and eigenvectors are used to analyse the system.

$$\delta f_q = \frac{1}{2}\mathbf{v}^T\cdot\mathbf{M}_q\cdot\mathbf{v}, \qquad (11)$$

$$\mathbf{v}^T = \left[(u_q)_r, (u_q)_i, (\bar{h}_q)_r, (\bar{h}_q)_i, (\delta\tilde{m}_q^+)_r, (\delta\tilde{m}_q^+)_i, (\delta\tilde{m}_q^-)_r, (\delta\tilde{m}_q^-)_i\right]$$

$$M_q = \begin{bmatrix} M_{11} & 0 & M_{12} & 0 & 0 & M_{13} & 0 & -M_{13} \\ 0 & M_{11} & 0 & M_{22} & -M_{13} & 0 & M_{13} & 0 \\ M_{12} & 0 & M_{22} & 0 & 0 & M_{13} & 0 & M_{13} \\ 0 & M_{12} & 0 & M_{22} & -M_{13} & 0 & -M_{13} & 0 \\ 0 & -M_{13} & 0 & -M_{13} & M_{33} & 0 & 0 & 0 \\ M_{13} & 0 & M_{13} & 0 & 0 & M_{33} & 0 & 0 \\ 0 & M_{13} & 0 & -M_{13} & 0 & 0 & M_{33} & 0 \\ -M_{13} & 0 & M_{13} & 0 & 0 & 0 & 0 & M_{33} \end{bmatrix}$$

$$M_{11} = \hat{q}^4 + \left(\sigma_s - \sigma_p \frac{\phi^2}{\sigma_p^2 - \phi^2}\right)\hat{q}^2 + \sigma_A,\ M_{12} = \sigma_p^2 \hat{q}^2 \frac{\phi^2}{\sigma_p^2 - \phi^2}$$

$$M_{22} = \hat{q}^4 + \left(\sigma_s - \sigma_p \frac{\phi^2}{\sigma_p^2 - \phi^2}\right)\hat{q}^2,\ M_{13} = i\sigma_c \hat{q}^3,\ M_{33} = 2\sigma_\chi.$$

5 The Model

We want to create a model based on particles that reproduces the properties of systems which self-assemble into nearly 2D structures, forming solid-like and liquid like layers and bilayers. To reproduce electroporation, the model has to include the coupling of the particles with an external electric field. The starting point is provided by a model proposed in the literature a few years ago[1]. This model contains N particles with position vectors $\mathbf{r_1}, \ldots, \mathbf{r_N}$ and dipole vectors $\mathbf{S_1}, \ldots, \mathbf{S_N}$. The dipoles are of fixed, dimensionless length S with variable orien-

tation. The potential energy of the system is given by[4],

$$U = \frac{1}{2}\sum_{i\neq j}\epsilon\left[4\left(\frac{\sigma}{|\mathbf{r_{ij}}|}\right)^{12} - \sigma^3\left(\frac{\mathbf{S_i}\cdot\mathbf{S_j}}{|\mathbf{r_{ij}}|^3} - \frac{3(\mathbf{S_i}\cdot\mathbf{r_{ij}})(\mathbf{S_j}\cdot\mathbf{r_{ij}})}{|\mathbf{r_{ij}}|^5}\right)\right], \tag{12}$$

with $\mathbf{r_{ij}} = \mathbf{r_i} - \mathbf{r_j}$, (σ, ϵ) = length and energy scales and "$\cdot$" is the usual dot product of vectors. The first term in the square brackets represents a short range repulsive potential, preventing the collapse of the system. The **S**-dependent part of the potential is of the same form as the electrostatic dipole potential but with a crucial change of sign, so these particles are called anti-dipoles. The change of sign affects the dependence of the potential energy of particle pairs on the relative orientation of their dipoles, as illustrated in Fig. 5

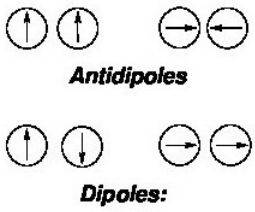

Figure 5: Low-energy configurations of dipoles and anti-dipoles.[a]

Looking at a locally planar structures, we see that a single layer of particles become stable when the dipoles are nearly parallel among themselves and perpendicular to the plane. The dipole contribution to the energy for these structures is then given by,

$$U_{dipole} = -\frac{1}{2}\sum_{i\neq j}\epsilon\sigma^3\left(\frac{\mathbf{S_i}\cdot\mathbf{S_j}}{|\mathbf{r_{ij}}|^3} - \frac{3(\mathbf{S_i}\cdot\mathbf{r_{ij}})(\mathbf{S_j}\cdot\mathbf{r_{ij}})}{|\mathbf{r_{ij}}|^5}\right) = U_3 + U_5,$$

with U_3 and U_5 for nearly parallel dipoles,

$$U_3 = -\frac{1}{2}\sum_{i\neq j} \epsilon\sigma^3 \left(\frac{\mathbf{S_i}\cdot\mathbf{S_j}}{|\mathbf{r_{ij}}|^3}\right) \sim -\frac{1}{2}|S|^2 \sum_{i\neq j} \epsilon \left(\frac{\sigma}{|\mathbf{r_{ij}}|}\right)^3,$$

$$U_5 = -\frac{1}{2}\sum_{i\neq j} \epsilon\sigma^3 \left(\frac{3(\mathbf{S_i}\cdot\mathbf{r_{ij}})(\mathbf{S_j}\cdot\mathbf{r_{ij}})}{|\mathbf{r_{ij}}|^5}\right) \sim 0,$$

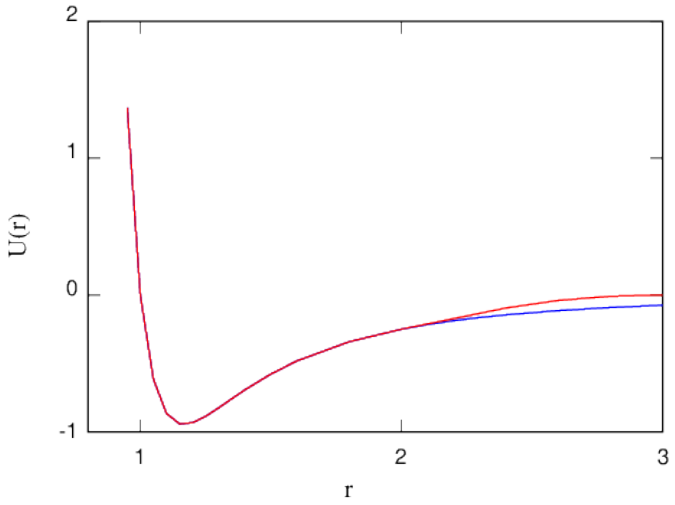

Figure 6: Distance dependence of the interaction of two particle moving in the xy plane with their dipoles parallel and oriented along z. Blue curve: long range version of the model: red curve: short range version of the model.

The distance dependence of the in-plane interaction of two anti-dipole particles whose **S** is parallel in shown by the blue curve in Fig 6. The lowest energy 2D configuration of particles whose pair interaction is the sum of a short range repulsion and a long range attractive tail is a compact hexagonal arrangement as shown in panel (a) of Fig. 7.

Strictly speaking, the original model[1] was developed to replace a bilayer by a single layer of anti-dipoles, whose two (+ and −) polarities representing the two

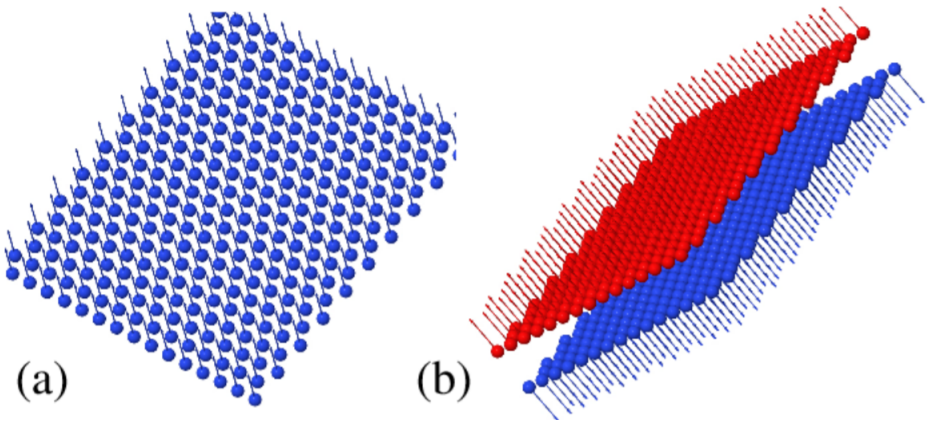

Figure 7: Snapshot of: (a) a single anti-dipole layer: (b) a bilayer. The blue and red colors are used to distinguish the particles belonging to the two leaflets. When $E_z = 0$, however, the two leaflets are completely equivalent.

leaflets. This mapping, however, does not allow to differentiate the two leaflets, that is instead required for a faithful model of electroporation. In my study, therefore, the mapping was modified in such a way to represent each leaflet by an anti-dipole layer. This is possible since pairs of planar layers can be approached to each other, feeling an attractive interaction provided their dipoles are oriented opposite to each other (See panel (b) of Fig. 7). The stability of the bilayer at short distance is ensured by the repulsive, dipole-independent term in the potential energy. The dependence of the system energy per particle on the inter-layer distance d_z is illustrated in Fig. 7.

In the original model, the dipole moment $\mathbf{S}$ is only a computational device to make the particles self-assemble into a nearly 2D geometry. In the present case, we take literally the dipole nature of $\mathbf{S}$, and we make it interact with an external electric field in the usual electrostatic way. Hence, in addition to the particle-particle and dipole-dipole interaction, the model includes the interaction of each dipole with an external electric field $\mathbf{E}$ of constant orientation and strength over

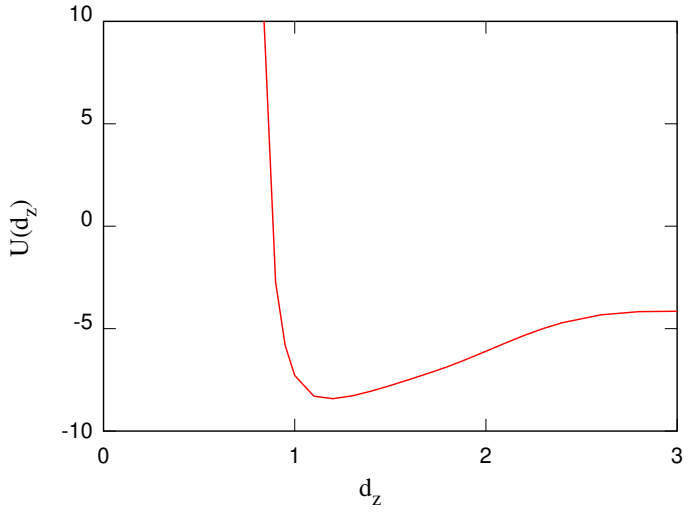

Figure 8: Dependence of the potential energy per particle of a bilayer on the separation d_z between the two leaflets.

the entire sample:

$$U_{Elec} = -\mathbf{E} \cdot \sum_{i=1}^{N} \mathbf{S_i} \tag{13}$$

Preliminary simulations have shown that this first models, whose dipole-dipole interactions are long-range, is unable to reproduce electroporation because the coupling among dipoles is too strong, resulting into a strongly collective behaviour that prevents the formation of localised holes. To correct this drawback, a short range variant of the anti-dipole model has been developed. This is obtained by multiplying the dipole-dipole part by a short range function $f_c(r)$:

$$U = \frac{1}{2} \sum_{i \neq j} \epsilon \left[4 \left(\frac{\sigma}{|\mathbf{r_{ij}}|} \right)^{12} - \sigma^3 f_c(r_{ij}) \left(\frac{\mathbf{S_i} \cdot \mathbf{S_j}}{|\mathbf{r_{ij}}|^3} - \frac{3(\mathbf{S_i} \cdot \mathbf{r_{ij}})(\mathbf{S_j} \cdot \mathbf{r_{ij}})}{|\mathbf{r_{ij}}|^5} \right) \right], \tag{14}$$

where:

$$f_c(r) = \begin{cases} 1 & \text{if } r \leq r_c \\ \left(1 - \cos \frac{2\pi r}{\Delta}\right) & \text{if } r_c \leq r \leq r_c + D \\ 0 & \text{otherwise} \end{cases} \tag{15}$$

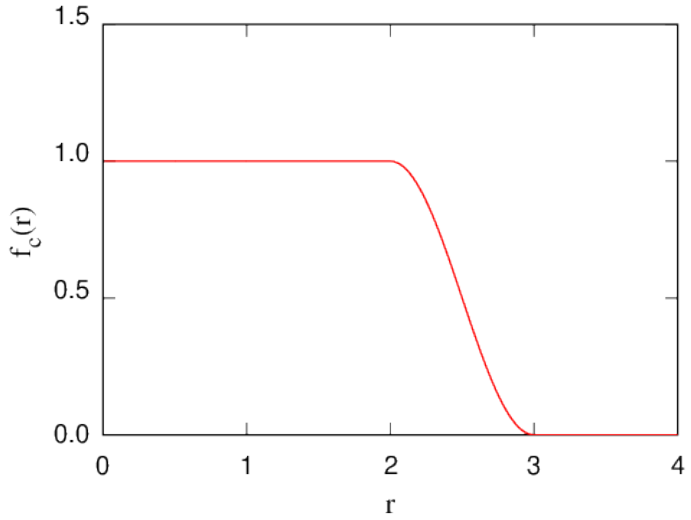

Figure 9: Cut-off function $f_c(r)$ introduce to limit the interaction range of anti-dipoles.

In this equation r_c is a cut-off distance for the interaction, D is the with of the spherical corona in which f_c turns from 1 to 0, being continuous everywhere with its first derivative. The radial dependence of f_c is illustrated in Fig. 9. The corresponding pair interaction is represented by the red curve in Fig. 6. Although the difference of the long- and short-range potentials appears rather minor on the figure, the effect of the long-range tail (blue curve) integrated over increasing areas is large. This short-range anti-dipole model is our primary candidate to simulate electroporation.

6 Units

In my study and in these reports, all quantities are expressed in scaled units. In other terms, I set the most important characteristic length and energy of the system to 1, in this case the ϵ and σ of the potential energy in Eq. 12. Moreover $|\mathbf{S}|$ is a dimensionless parameter deciding the relative strength of the repulsive and dipole-dependent interaction energy. These choices are sufficient to fix the units needed to express all quantities that we can compute by Monte Carlo. For completeness, it is worth pointing out that the set of units defined above does not define a time (or, equivalently, mass unit) that is not required in Monte Carlo but is relevant in molecular dynamics. To cover time units, we could set the mass of each particle equal to 1. Given the unit of energy, this is enough to fix the unit of time.

In this way, the model can be adapted to a wide variety of systems and conditions. To target any specific real system, it is enough to know what is the size of the real particles, their interaction energy and mass. Then, it is immediate to establish the correspondence between real and scaled units.

For instance, in the case of phospholipid bilayers relevant for biomembranes, the diameter of their polar head is of the order of 1nm (hence: $\sigma = 1$), their interaction energy is of the order of 0.1 eV (hence: $\epsilon = 0.1$ eV) and the mass of the single lipid is about a few hundred atomic mass units.

7 Method: Monte Carlo

The potential energy of an assembly of N anti-dipoles can be combined with the kinetic energy of the corresponding particles to give the system Hamiltonian:

$$H(\mathbf{P}, \mathbf{r}; \mathbf{S}) = \sum_{i=1}^{N} \frac{\mathbf{P^2}}{2m} + U[\mathbf{r}; \mathbf{S}] \tag{16}$$

where $\{\mathbf{P}^N\}$ are the particles' momenta, m is their mass, and U is the potential energy of anti-dipoles given in Eq. 11. Given suitable initial conditions, the Hamiltonian H gives the time evolution of the system, which is in fact the most detailed information we can get. However, since we deal with samples made of thousands of particles, such detail is not very useful. We are more interested in the statistical properties of the system at thermal equilibrium at time T. To investigate these properties, we first define the phase space Ω of the system, consisting of all combinations of coordinates (including spins) and momenta that particles can take. In other terms, $\Omega = \{\mathbf{P}^N\} \otimes \{\mathbf{r}^N\} \otimes \{\mathbf{S}\}^N$. Each point on this space represents a state (defined by coordinates and momenta) admissible for our system. At thermal equilibrium, there will be a well defined probability distribution over the phase space $\mathcal{P}(\mathbf{P}^N; \mathbf{r}^N; \mathbf{S}^N)$ giving the probability of finding the system in any state defined by coordinates and momenta. Once $\mathcal{P}$ is known, the thermal average $\langle A(\mathbf{P}^N; \mathbf{r}^N; \mathbf{S}^N)\rangle$ of a generic operator $A(\mathbf{P}^N; \mathbf{r}^N; \mathbf{S}^N)$ dependent on the particles' momenta and coordinates can be computed as:

$$\langle A(\mathbf{P}^N; \mathbf{r}^N; \mathbf{S}^N)\rangle = \int \mathcal{P}(\mathbf{P}^N; \mathbf{r}^N; \mathbf{S}^N) A(\mathbf{P}^N; \mathbf{r}^N; \mathbf{S}^N) d\Omega \tag{17}$$

where $d\Omega$, volume element in phase space, is:

$$d\Omega = d\mathbf{p}^N d\mathbf{r}^N d\mathbf{S}^N \tag{18}$$

Of course, Eq. 17 requires $\mathcal{P}(\mathbf{P}^N; \mathbf{r}^N; \mathbf{S}^N)$ to be normalised:

$$\int \mathcal{P}(\mathbf{P}^N; \mathbf{r}^N; \mathbf{S}^N) d\Omega = 1 \tag{19}$$

According to Boltzmann theory:

$$\mathcal{P}(\mathbf{P}^N; \mathbf{r}^N; \mathbf{S}) = \frac{e^{-\beta H(\mathbf{P},\mathbf{r};\mathbf{S})}}{Q_N} \tag{20}$$

where $\beta = 1/k_B T$, k_B being the Boltzmann constant. Moreover, Q_N is the partition function. Because of Eq. (19):

$$Q_N = \int e^{-\beta H(\mathbf{P},\mathbf{r};\mathbf{S})} d\Omega \tag{21}$$

Hence, while the numerator in Eq. 20 is easy to compute, the denominator is virtually impossible to determine, since it is expressed by a multidimensional integral. These considerations seem to rule out any practical usage of Eq. 17. However, an algorithm, i.e., Monte Carlo, has been proposed and progressively developed into a major statistical mechanics approach to compute thermal averages integrating over the probability distribution in phase space, even though this function is never computed explicitly. The strategy of MC relies on the generation of a sequence of M configurations ($i = 1, ..., M$) in phase space, whose eventual distribution reproduces the Boltzmann function of Eq. 20. Hence, every thermal average (see Eq. 21) can be computed simply as an average over the configurations in the sequence. The choice of configuration $(i + 1)$ in the sequence depends only on configuration i (Markov chain), and is carried out through the following steps.

- Starting with configuration i of energy E_i, a particle ia is selected at random

- The coordinates of particle ia are changed by a (relatively small) random displacement $\delta\mathbf{q}$
- The energy E_{new} of the new configuration is computed
- If $E_{new} \leq E_i$, the new configuration is accepted, becoming configuration $(i+1)$ of energy $E_{i+1} = E_{new}$
- If $E_{new} > E_i$, the new configuration is accepted with probability $e^{-\beta(E_{new}-E_i}$, otherwise the displacement of particle ia is rejected. In such a case, configuration $(i+1)$ will be the same of configuration i, and $E_{i+1} = E_i$.

This sequence of operations/decisions represents a MC step, and is repeated many times (typically $10^6 - 10^7$) to generate a sequence of configurations long enough to compute thermal averages. More precisely, since the property of the Markov chain to approach the Boltzmann distribution develops only after a first stage of sampling, our simulations will consist of two parts. The first one is required to equilibrate the system at the selected T, the second represents the production stage, in which statistics for all relevant quantities is accumulated.

8 Creating the model

We used C++ to create the model of N particles, with 2 layers in the xy plane, one with their spins parallel to the z-axis, and the other with them anti-parallel to the z-axis. The unit cell has length S_x and width S_y. First, we create position vectors, $\mathbf{r_1}...\mathbf{r_N}$, for each particle, and their corresponding spin vectors, $\mathbf{S_1}...\mathbf{S_N}$, which are stored in another vector L. So L is a vector of vectors, which is like a $6 \times N$ matrix, for N particles with row i equal to the x, y and z coordinates of the

vectors $\mathbf{r_i}$ and $\mathbf{S_i}$.

$$L = \begin{bmatrix} \mathbf{r_1} & \mathbf{S_1} \\ ... & ... \\ \mathbf{r_N} & \mathbf{S_N} \end{bmatrix}$$

We define a function $U_{ij}(\mathbf{r_i}, \mathbf{S_i}, \mathbf{r_j}, \mathbf{S_j})$ to return the potential energy between particles i and j using the antidipole formula. Then we define a function $U_{total}(L)$ to return the total potential energy of a bilayer described by the vector L, by summing the potential of all pairs of particles in L. We must also inclued the boundary conditions in this function. To do this, we treat every particle as if its in the middle of the unit cell, so when calculating the potential between particles i and j, if the difference in their x coordinates, $x_j - x_i$, is greater than half the length of the unit cell, $S_x/2$, we move particle j to the left by the distance S_x. So its x coordinate becomes $x_{new} = x_{old} - S_x$. If $x_j - x_i < -S_x/2$, then $x_{new} = x_{old} + S_x$. We do the same for the y coordinates, if $y_j - y_i > S_y/2$, then $y_{new} = y_{old} - S_y$, if $y_j - y_i < -S_y/2$, then $y_{new} = y_{old} + S_y$. We then add the interaction of the particles with an electric field, $U_{Elec}(L) = -\mathbf{E} \cdot \sum \mathbf{S_i}$, so the total energy of the bilayer represented by L bceomes $E = U_{total}(L) + U_{Elec}(L)$.

Monte Carlo Simulation:

L represents one configuration on the configuration phase space, Ω. Using a random number generator, starting with the configuration L with energy E, a particle is selected at random, moved by a random displacement, and the energy of the new configuration is calculated, $E_{new} = U_{total}(L_{new}) + U_{Elec}(L_{new})$. If $E_{new} < E_{old}$, the move is accepted. If $E_{new} > E_{old}$, produce a random number h and if $h < e^{-\beta(E_{new} - E_{old})}$, the move is accepted. Otherwise the move is rejected. Then another particle is selected at random, its spin is rotated by a random angle, and the new energy is calculated for this configuration. This move is accepted

with the same conditions described above. These two processes are one step in the Monte Carlo simulation, which are repeated $\sim 10^7$ times. The first half of the simulation is required to bring the simulated sample in a state of thermal equilibrium. This part of the trajectory is discarded, and the average of all properties is computed on the remaining steps.

9 Analysis of trajectories

After each step in the Monte Carlo process, a snapshot of the coordinates, spin and average potential energy per particle is taken. Although MC does not follow Newton's equations of motion, the sequence of these snapshots is called the system trajectory for each simulation. We use these trajectories to calculate the density distribution of particles along the z-axis (which should have 2 peaks corresponding to each leaflet in the bilayer), the in-plane radial distribution function(which describes the distribution of particles in each leaflet) and the heigh-height correlation as a function of temperature and electric field (which describes the flatness of each leaflet). These quantities are calculated as follows,

Density along z: $\rho(z)$

We consider z in the range $z = -3$ to $z = 3$, covered by 120 bins each 0.05 wide (in scaled units). We initialise a vector h consisting of 120 0's. We define the bin index as $ind = z/0.05$ and for each particle we increase $h[ind]$ by 1, giving us a histogram of the z coordinates of the particles.

In-plane radial distribution function: $g(r_n)$

This concerns the distribution of neighbours around a central particle within each plane. In this case we take 201 bins of width 0.05. We set a vector hr equal to 201 0's. We take a particle i and all other particles j belonging to the same plane, and compute the in-plane distance

$dr_{ij} = \sqrt{(x_i - x_j)^2 + (y_i - y_j)^2}$. For each j, we calculate $ind = dr_{ij}/0.05$ and increase $hr[ind]$ by 1. We repeat this process taking every particle as the central particle i, and we average.

The area of bin "n", covering from $r_n = 0.05n$ to $r_{n+1} = 0.05(n+1)$ is $dA_n = \pi(r_{n+1}^2 - r_n^2)$. To provide a histogram corrected for the increase in counts due to the increasing area, we calculate $g(r_n) = hr(n)/dA_n$.

Height-height correlation function: $hzhz(r)$

We set two vectors hz and nz both equal to 201 0's. Again, we select a particle i and compute dr_{ij} and $ind = dr_{ij}/0.05$ for all particles j in the same plane. We increase $hz[ind]$ by $dz = |z_j - z_i|$ and $nz[ind]$ by 1. We repeat this process taking every particle as the central particle i, and we average. We calculate $hz[n]/nz[n]$. This is the average separation of particles whose in-plane distance is $0.05n$. If each layer is perfectly flat, the function vanishes at all distances. If the layers are rough, this quantity will be large, increasing nearly monotonically with distance. The function will be small at short distances because neighbouring particles on the same plane will not be separated by large z values.

10 Results

Computations have been carried out by MC on systems consisting of $N = 2400$ particles, based on the short-range version of the anti-dipole model. At the beginning of the simulations, particles have been arranged on two parallel planes oriented along the xy plane, at a distance along z of 1.5 distance units. Within each plane, particles occupy the lattice positions of the compact hexagonal structure at a nearest neighbour distance $r_0 \sim 1.2$ that minimises the system energy. As anticipated in the model section, the dipoles of particles on the same plane are parallel, and antiparallel to the dipoles on the opposite plane. To reduce finite-size

effects, the sample is periodically replicated in 2D. To accommodate the compact hexagonal structure, the periodicity is set to $s_x = 30$ and $s_y = 34.64$, again in scaled units. Two series of simulations have been performed, each representing a scan in temperature $0.3 \leq T \leq 2.$. The first series has $E_z = 0$, the second series instead covers a wide range of applied electric fields up to the electroporation threshold $E_z = 2$. Each simulation, corresponding to a choice of T and E_z values, consists of 4×10^6 MC steps of equilibration, and 6×10^6 MC steps of statistics. Each step corresponds to the attempted displacement of one particle selected at random, and to the attempted change of orientation of the dipole of another particle, also selected at random. The amplitude of the attempted displacements is tuned in such a way that the acceptance ratio of displacements and vector rotations is between 0.3 and 0.5. Since the acceptance ratio increases with increasing T, the attempted displacements are also progressively increase with increasing T. During the simulations we compute the average potential energy per particle, and we store a sequence of snapshots, i.e., the system *trajectory* during the simulation. Since MC does not follow Newton's equations of motion, the trajectory cannot be seen as representing the system dynamics. Nevertheless, quantities such as the diffusion rate in phase space (which is not the experimental diffusion coefficient) can be extracted. A posteriori, trajectories are displayed in a movie form by standard visualisation tools such as Jmol or VMD. Visual inspection of these movies provides the first way to assess the stability of bilayers under an external field of increasing strength. Moreover, trajectories are analysed to compute the average density distribution along z, the in-plane radial distribution function, the height-height correlation as a function of temperature and electric field. The simulations at $E_z = 0$ show that the bilayer is remarkably stable up to $T = 2$. The average potential energy per particle grows nearly linearly with increasing T, pointing

to a nearly constant specific heat (See Fig. 10). At low T ($T \leq 1$) the value of $C = \partial U/\partial T$ is remarkably close to $\frac{5}{2}k_B$, as expected of a harmonic solid in which each particle is described by five degrees of freedom (three translation, and two orientational degrees of freedom). The broad anomaly at $T \sim 1.3$ corresponds to the $2D$ melting of the bilayer. Above T_m, therefore, a bilayer of anti-dipoles is a 2D liquid, enhancing its correspondence with the real system, since lipid bilayers and biomembranes in particular are liquid-like at physiological conditions.

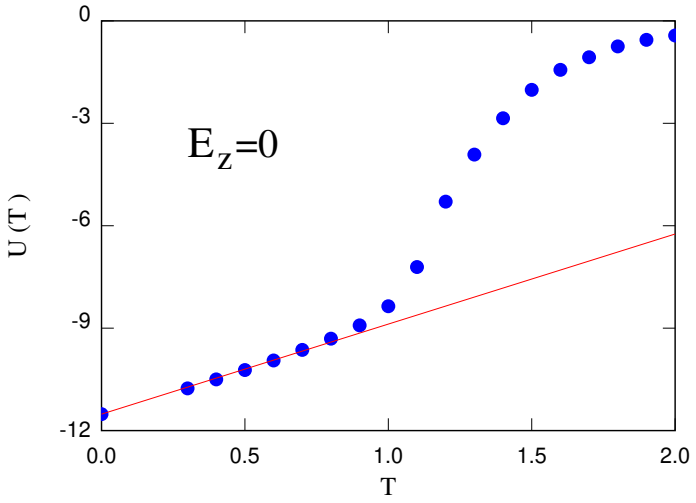

Figure 10: Temperature dependence of the average potential energy of a bilayer at $E_z = 0$. The red line, whose slope is $C = 2.52$ is a linear interpolation of the low-T part of $U(T)$.

The temperature dependence of the particle density along z is shown in Fig. 11 Up to (at least) $T = 1.2$ the bilayer remains flat, as can be seen in Fig. 12., showing the height-height correlation function $\langle hzhz(r)\rangle$ as a function of the logarithm of r, computed at four different temperatures. In all these cases, the correlation function tends to a constant value. According to the accepted statistical mechanics definition, at all these temperatures the bilayer is thermodynamically flat, al-

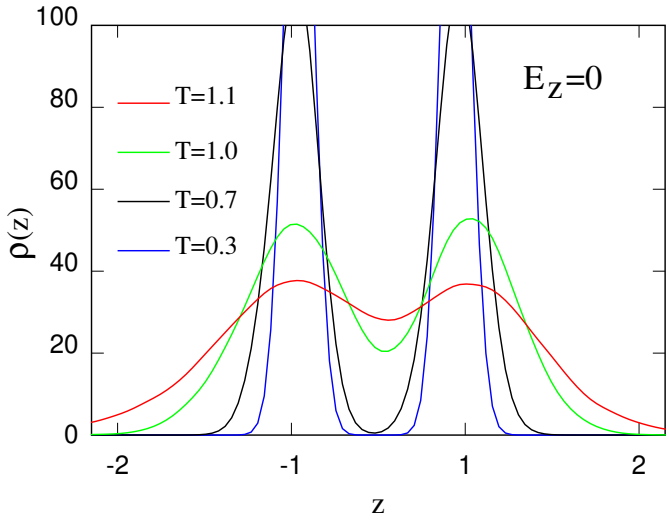

Figure 11: Temperature dependence of the density profile along z.

though the mean square fluctuation of the bilayer height, given by the asymptotic value of the correlation function, increases rapidly with increasing T.

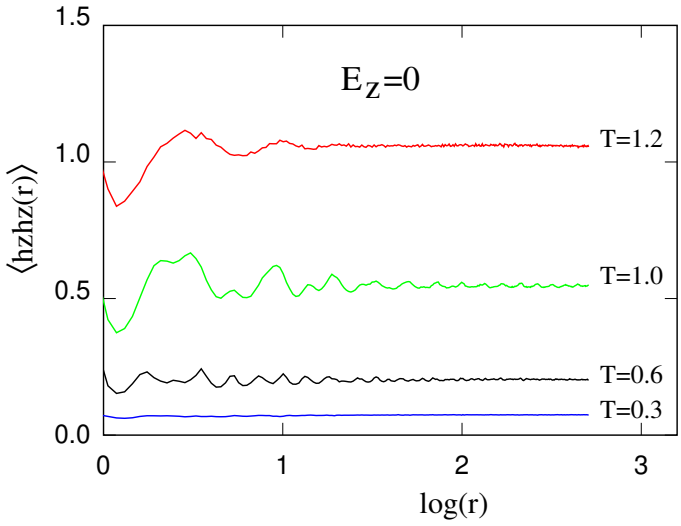

Figure 12: Temperature dependence of the height-height correlation function. The radial distance r is reported on a logarithmic scale.

The addition of an external electric field changes the relative stability of the two leaflets in the bilayer, since the leaflet whose dipoles are parallel to the external field will increase its stability, while the leaflet whose dipoles are anti-parallel to the external field will be destabilized. This is already apparent from a plot of the particle density $\rho(z)$ (See Fig. 12), showing that the application of the external field progressively destabilises one of the two leaflets.

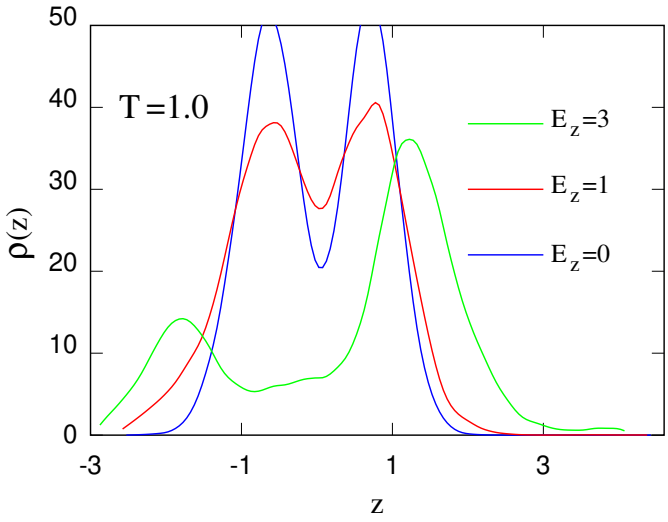

Figure 13: Density distribution along the direction z orthogonal to the bilayer for samples at $T = 1.0$ under an external electric field of increasing strength. The peak on the left corresponds to the leaflet whose dipoles are anti-parallel to E_z, while the peak on the right corresponds to the leaflet whose dipole are parallel to E_z.

The process of dissolving the leaflet whose dipoles are anti-parallel to the applied field can be followed in the simulation trajectories. Three snapshots fromthe simulation at $T = 1.0$, $E_z = 2.0$ are given in Fig. 14. The first snapshot (a) refers to the beginning of the simulation after adding the external field. The following snapshots show the same system after: (b) 2×10^6 and (c) 4×10^6 MC steps, documenting the formation of holes in the unstable leaflet.

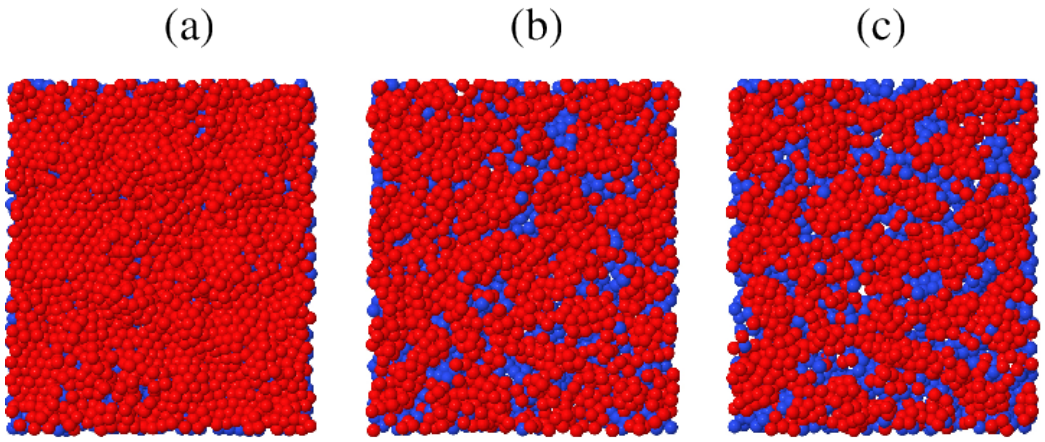

Figure 14: Snapshots from a simulation at $T = 1.0$, $E_z = 2.0$. (a) First configuration following the application of the $E_z = 2.0$ field on a sample equilibrated at $T = 1.0$, $E_z = 0$; (b) configuration 2×10^6 MC steps after (a); (c) configuration 2×10^6 MC steps after (b).

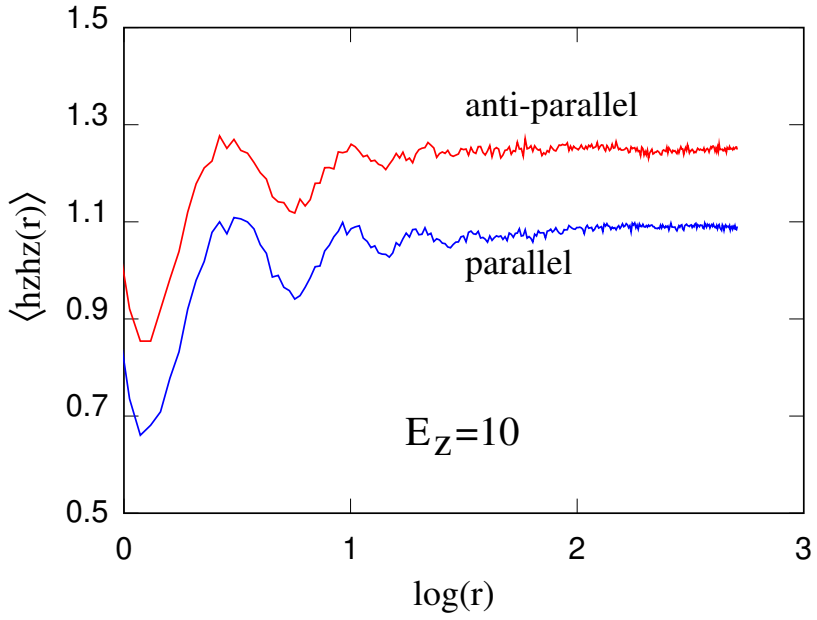

Figure 15: Height-height correlation function computed for the two leaflets in the case $E_z = 10$.

The unequal effect of the external field on the two leaflets is apparent also by comparing the height-height correlation function for the two leaflets. While in the $E_z = 0$ case the two functions are the same apart from statistical fluctuations, they differ substantially in the $E_z \neq 0$ case. This is shown in Fig. 15, comparing the height-height correlation function in the $E_z = 2$ case. Although both leaflets are still thermodynamically smooth, the mean square fluctuation in the z-coordinate of the leaflet with anti-parallel spins is greatly enhanced, since its stability is decreased by the external field.

The comparison of the structure of the two leaflets at an intermediate stage of the hole formation is shown in Fig. 16.

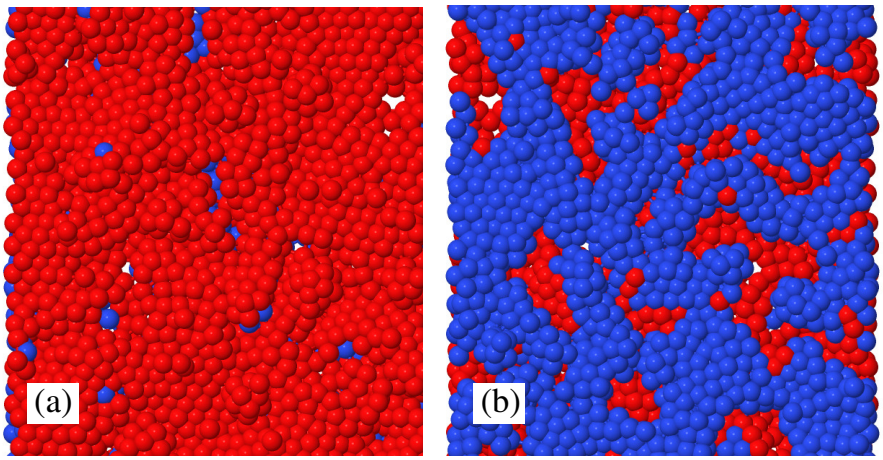

Figure 16: The side of the bilayer: (a) stabilised by the external electric field; destabilised by the external electric field.

11 Summary and Conclusions

The project aimed at developing and testing a model based on particles able to reproduce electroporation of lipid bilayers under an external electric field, suitable to be applied in computer simulations using either Monte Carlo or molecular

dynamics. The long term goal is to analyse by simulation the role of the various model parameters in the onset and time evolution of electroporation, and to investigate the effect of chemical additives that could be used for biomedical applications.

During the first semester of my project, I studied the literature on electroporation, and especially on theoretical and computational studies of this phenomenon. I also reproduced the results of a theoretical study using an approximate free energy functional to model electroporation. In the second semester I developed a model of bilayers closely related to the anti-dipole model proposed in the literature. The model is heavily coarse-grained but still based on particles which carry a dipole, and are arranged on two neary planar layers (leaflets), separated by a distance d comparable to the inter-molecular distance. The dipoles on particles belonging to different leaflets are anti-parallel. The particle-particle interaction is short range, two-body but dependent on the orientation of the dipole of the two interacting particles. The dipole carried by the particles may interacts with any external field applied to the system. The dependence of the particle-particle interaction on the orientation of their dipoles is the crucial ingredient that makes the model able to reproduce electroporation. During the project, I validated this model by a series of Monte Carlo simulations been carried out by Monte Carlo, both in the absence and in the presence of an external field perpendicular to the average plane of the bilayer.

Analysis of trajectories shows that in the absence of an external field the bilayer is stable over a fairly extended range of temperatures. The properties have been characterised by looking at animations of the simulation trajectory, and by computing a variety of structural properties such as the density distribution along the direction normal to the bilayer, the radial distribution functions, the height-

height correlation function. The model displays a (2D) solid-liquid transition, corresponding to the onset of long range diffusion of particles. This transition is very important, since real biomembranes are liquid-like at physiological conditions. At higher temperature particles evaporate from the bilayer at a rate that increases with increasing T. Both in the solid-like and in the liquid-like phase, the thermal undulations of the bilayer become increasingly important with increasing T. However, the height-heigh correlation function saturates to a constant at all simulated T, showing that the bilayer is thermodynamically smooth over the entire temperature range that we simulated.

Since at low T dipoles on the same leaflet are parallel to each other, and anti-parallel to dipoles on the other leaflet, the total dipole moment of the bilayer is low, and the application of an external field at first has a negligible effect. With increasing T and/or E_z, however, the leaflet whose dipoles are anti-parallel to E_z is progressively destabilised, shedding particles at an increasing rate.

This phenomenon is similar to what happens in the first stages of electroporation. In this respect, therefore, the model is successful. However, the destabilisation of the second leaflet, which is part of real electroporation is not observed in the simulations. It is easy to trace this limitation to the fact that isolated leaflets are stable in the model, contrary to what happens in reality. Correcting this problem is easy, and it will be done at a later stage.

Already at this stage, however, it is apparent that the model could become a standard tool for coarse grained simulations of electroporations. A model of this kind has never been proposed in the literature, and could instead be applied to investigate electroporation covering several length scales.

The model could be used also in molecular dynamics simulations, extending its reach also to different time scales.

References

[1] M. G. Del Pópolo and P. Ballone, *J. Chem. Phys.* 128, 024705 (2008).

[2] E. Neumann et al., *The EMBO Journal* 1 (7), P841–845 (1982).

[3] T. Kotnik et al., *Trends in Biotechnology* Vol. 33, No. 8, P480-488 (2015).

[4] J. T. Sengel and M. I. Wallace, *PNAS* Vol. 113, No. 19, P5281-5286 (2016).

[5] T. Kotnik et al., *Annual Review of Biophysics* Vol. 48, P63-91 (2019).

[6] S.J. Marrink, E. Lindahl, O. Edholm, A.E. Mark, *J. Am. Chem. Soc.* 123, P8638–8639 (2001)

[7] D.P. Tieleman, H. Leontiadou, A.E. Mark, S.J. Marrink, *J. Am. Chem. Soc.* 125, P6382–6383 (2003)

[8] M. Pavlin et al., *Advances in Planar Lipid Bilayers and Liposomes* 6, P167-219 (2008)

[9] D. H. Michael and M. E. O'Neill, *J. Fluid. Mech.* 41, P571-580 (1970).

[10] G. I. Taylor and D. H. Michael, *J. Fluid. Mech.* 58, P625-639 (1973).

[11] J. M. Crowley, *Biophysics. J.* 13, P118-143 (1973).

[12]] C. Maldarelli, R. K. Jain, I. B. Ivanov, E. Rckenstein, *J. Colloid Interface Sci.* 78, P118-143, (1980)

[13] A. Steinchen, D. Gallez, A. Sanfeld, *, J. Colloid Interface Sci.* 85, P5-15, (1982).

[14] I. P. Sugár, *Biochim. Biophys. Acta* 556, P72-85 (1979).

[15] R. J. Bingham and P. D. Olmsted, *Physical Review* E 81, 051909 (2010).